Published in final edited form as:
Cell. 2015 January 29; 160(3): 407–419. doi:10.1016/j.cell.2015.01.010.

A ribonuclease coordinates siRNA amplification and mRNA cleavage during RNAi

Hsin-Yue Tsai[1,3], **Chun-Chieh G. Chen**[1], **Darryl Conte Jr**[1], **James J. Moresco**[4], **Daniel A. Chaves**[1,5], **Shohei Mitani**[6], **John R. Yates III**[4], **Ming-Daw Tsai**[3], and **Craig C. Mello**[1,2]

[1]RNA Therapeutics Institute, University of Massachusetts Medical School, Worcester, MA 01605, USA

[2]Howard Hughes Medical Institute, University of Massachusetts Medical School, Worcester, MA 01605, USA

[3]Institute of Biological Chemistry, Academia Sinica, Nankang, Taipei 115, Taiwan

[4]Department of Chemical Physiology, The Scripps Research Institute, La Jolla, CA 92037, USA

[5]Instituto de Medicina Molecular, Faculdade de Medicina, Universidade de Lisboa, Avenida Professor Egas Moniz, 1649-028 Lisboa, Portugal

[6]CREST, Japan Science and Technology Agency and Department of Physiology, Tokyo Women's Medical University School of Medicine, Tokyo 162-8666, Japan

SUMMARY

Effective silencing by RNA-interference (RNAi) depends on mechanisms that amplify and propagate the silencing signal. In some organisms, small-interfering (si) RNAs are amplified from target mRNAs by RNA-dependent RNA polymerase (RdRP). Both RdRP recruitment and mRNA silencing require Argonaute proteins, which are generally thought to degrade RNAi targets by directly cleaving them. However in *C. elegans*, the enzymatic activity of the primary Argonaute, RDE-1, is not required for silencing activity. We show that RDE-1 can instead recruit an endoribonuclease, RDE-8, to target RNA. RDE-8 can cleave RNA in vitro and is needed for the production of 3′ uridylated fragments of target mRNA in vivo. We also find that RDE-8 promotes RdRP activity, thereby ensuring amplification of siRNAs. Together, our findings suggest a model in which RDE-8 cleaves target mRNAs to mediate silencing, while generating 3' uridylated mRNA fragments to serve as templates for the RdRP-directed amplification of the silencing signal.

ACCESSION NUMBERS

Illumina data are available from GEO under the accession number GSE59300

SUPPLEMENTAL INFORMATION

Supplemental Information includes Extended Experimental Procedures, six figures, and three tables and can be found with this article online.

INTRODUCTION

RNA interference (RNAi) is an ancient gene-silencing mechanism that employs evolutionarily conserved ribonuclease proteins called Argonautes. Argonautes achieve sequence-specific targeting through association with small RNA guides of ∼20–30 nucleotides (for review see Ghildiyal and Zamore, 2009). Pathways related to RNAi are as diverse as the organisms in which they are found and regulate a remarkable array of biological phenomena (Castel and Martienssen, 2013; Conine et al., 2013; Seth et al., 2013).

In *C. elegans*, RNAi triggered by foreign double-stranded (ds) RNA (referred to herein as exo-RNAi) is a two-step Argonaute response (Yigit et al., 2006). The primary Argonaute RDE-1 is loaded with siRNAs processed from dsRNA by the ribonuclease III-related enzyme Dicer (DCR-1). Target recognition by RDE-1/siRNA complexes initiates the amplification of antisense secondary siRNAs, which are synthesized de novo by RNA-dependent RNA polymerase (RdRP) and are primarily 22 nt with a 5′-triphosphorylated guanosine (22G-RNAs; Gu et al., 2009; Pak and Fire, 2007; Sijen et al., 2001; Sijen et al., 2007). Secondary siRNAs are loaded onto a family of worm-specific Argonautes (WAGOs), which lack catalytic-site metal-coordinating residues and thus mediate silencing through an unknown mechanism (Yigit et al., 2006). WAGOs include cytoplasmic and nuclear members that also function in multiple endogenous small RNA pathways to silence transposons, cryptic or aberrant genes, and foreign sequences (Gu et al., 2009; Guang et al., 2010; Guang et al., 2008; Shirayama et al., 2012; Yigit et al., 2006).

Endogenous small RNA pathways in *C. elegans* can be classified by their dependence on a primary Argonaute. For example, the Piwi ortholog PRG-1 uses genomically encoded piRNAs (21U-RNAs; Batista et al., 2008; Das et al., 2008; Ruby et al., 2006) to recognize targets with incomplete base-pairing complementarity and initiate a stable and heritable mode of epigenetic silencing known as RNAe (Ashe et al., 2012; Bagijn et al., 2012; Buckley et al., 2012; Lee et al., 2012; Shirayama et al., 2012). The maintenance of RNAe does not require PRG-1 activity but rather depends on RdRPs and both nuclear and cytoplasmic WAGOs, as well as chromatin factors (Ashe et al., 2012; Buckley et al., 2012; Lee et al., 2012; Shirayama et al., 2012). How the small RNA amplification machinery recognizes RNAe targets to maintain 22G-RNA levels at each generation remains unknown.

The ERI (for enhanced RNAi; Kennedy et al., 2004) pathway is a two-step Argonaute pathway that directly competes with the exo-RNAi pathway for available WAGOs (Duchaine et al., 2006; Gent et al., 2010; Vasale et al., 2010; Yigit et al., 2006). The ERI pathway requires both an RdRP (RRF-3) and DCR-1 to generate 26-nt siRNAs with a 5′-monophosphorylated G (Duchaine et al., 2006; Pavelec et al., 2009; Ruby et al., 2006; Vasale et al., 2010). The 26G-RNAs are loaded onto the Argonaute ERGO-1. Targeting by ERGO-1/26G-RNAs initiates 22G-RNA biogenesis by RdRPs (RRF-1 and EGO-1) and silencing by nuclear and cytoplasmic WAGOs (Gent et al., 2010; Guang et al., 2008; Vasale et al., 2010).

Here we describe a previously uncharacterized RNAi-deficient mutant, *rde-8*. RDE-8 protein contains a ribonuclease domain known as an N4BP1, YacP Nuclease (NYN) domain

(Anantharaman and Aravind, 2006) and is related to the Zc3h12a ribonuclease (Matsushita et al., 2009). We show that RDE-8 is required for the accumulation of two classes of RdRP-dependent small RNAs: RRF-1–dependent 22G-RNAs and RRF-3–dependent 26G-RNAs. We further show that RDE-8 is required for efficient RRF-1 RdRP activity in vitro. Using RNA immunoprecipitation (RIP), we show that RDE-8 associates with target mRNAs during exo-RNAi in an RDE-1–dependent but RdRP–independent manner. We identify RDE-8 homologs and RNAi and transposon-silencing factors as RDE-8–interacting proteins, and show that RDE-8 localizes to germline Mutator foci. Using 3′ rapid amplification of cDNA ends (RACE), we show that RDE-8 promotes the accumulation of target mRNA fragments tailed with untemplated 3′ uridine residues. Our findings are consistent with a role for RDE-8 both in mediating mRNA cleavage and promoting amplification of the silencing signal.

RESULTS

rde-8 encodes a NYN-domain ribonuclease

In a genetic screen for worms with an RNAi-deficient (Rde) phenotype, we isolated three independent alleles (*ne3309*, *ne3360*, and *ne3361*) of a gene we have named *rde-8*. In addition to the RNAi-deficient phenotype (Figure 1A), we observed a slight developmental delay, increased sensitivity to Orsay virus infection, and germline-transgene desilencing in *rde-8(ne3361)* (Figure S1). Using single-nucleotide polymorphisms and 3-factor analyses, we mapped the *rde-8* gene to a small interval on chromosome IV. Sequencing of candidate genes within this interval, revealed that all three alleles harbor the same single-nucleotide (nt) substitution in exon IV of the gene *ZC477.5*, resulting in a nonsense mutation at tryptophan 189 (Figure 1B). Western blot analyses failed to detect the RDE-8 protein in *rde-8(ne3361)* lysates (Figure 1C), suggesting that *ne3361* is a null or strong loss-of-function allele. Two deletion alleles of *rde-8* (*tm2252* and *tm2192*) that remove all or part of exons 4, 5, and 6 (Figure 1B) exhibited an Rde phenotype and failed to complement *rde-8(ne3361)* (data not shown). Finally, an integrated single-copy *gfp::ZC477.5* transgene rescued the Rde phenotype of *rde-8(ne3361)* (Figure 1A and S1). These data identify *ZC477.5* as *rde-8*.

RDE-8 is predicted to encode a 339 amino-acid protein homologous to prokaryotic, archaeal, and eukaryotic NYN-domain ribonucleases (Figure 1B; Anantharaman and Aravind, 2006). Notably, *gfp::rde-8* transgenes bearing mutations in conserved aspartic acid residues (either D76N alone or D145A and D146A together) that map to the catalytic site of Zc3h12a failed to rescue the Rde phenotype of *rde-8(ne3361)* (Figure 1A and data not shown). Western blot analysis of RDE-8 revealed that the expression of GFP::RDE-8(D76N) protein is comparable to endogenous RDE-8 and wild-type GFP::RDE-8 (Figure 1C). These findings suggest that an intact catalytic domain is required for RDE-8 activity.

To directly test whether RDE-8 encodes a ribonuclease, we purified recombinant, histidine-tagged RDE-8(WT) and RDE-8(D76N) proteins by nickel-chelating resin, anion-exchange, and gel-filtration chromatography (Figure 1D). We incubated recombinant RDE-8(WT) or RDE-8(D76N) proteins with an internally labeled 116-nt single-stranded RNA using

conditions that support in vitro Zc3h12a nuclease activity (Matsushita et al., 2009). RDE-8(WT) degraded the RNA substrate into variable size fragments, with prominent products of approximately 20 nt and 30 nt (Figure 1E). These products did not accumulate in reactions with recombinant RDE-8(D76N). Instead, an ∼85-nt product accumulated in the RDE-8(D76N) reactions and to much lower levels in RDE-8(WT) reactions. This product could represent an intermediate or, alternatively, the product of a bacterial nuclease contaminating the RDE-8 preparations. These data indicate that RDE-8 encodes an endoribonuclease required for RNAi.

RDE-8 is required for the accumulation of RdRP-dependent small RNAs

To explore where RDE-8 functions in the RNAi pathway, we examined small RNA production in mutant and wild-type *rde-8* transgenic strains exposed to dsRNA targeting the nonessential gene *sel-1* (Figure 2). Northern blot analysis revealed that *sel-1* siRNAs were reduced in *rde-8(ne3361)* relative to wild type (Figure 2A) and were rescued in *gfp::rde-8(+)* but not in *gfp::rde-8(D76N)* transgenic animals (Figure 2A and B). The microRNAs *let-7* and *miR-66* were unaffected and serve as loading controls (Figure 2A and B). We also cloned and deep sequenced small RNAs from *rde-8(ne3361)* mutants expressing *gfp::rde-8(+)* or *gfp::rde-8(D76N)* and exposed to *sel-1(RNAi)*. Consistent with the Northern blot data, we detected secondary siRNAs 5′ of the trigger in *gfp::rde-8(+)* worms after 8 hr of exposure to *sel-1* dsRNA, but not in the *gfp::rde-8(D76N)* mutant sample (Figure 2C). By 24 hours, *sel-1* siRNAs throughout the transcript were more abundant in the WT sample than in the *rde-8* mutant sample (Figure 2C). Thus, the RNAi defect of *rde-8* mutants correlates with failure to accumulate RdRP-derived siRNAs.

We also monitored the effect of *rde-8* on the accumulation of endogenous 22G-RNAs (Figure 2D and Figure S2). We found that 22G-RNAs were reduced at least 2-fold in the *rde-8*(*ne3361*) mutant for 42% (n=4632) of genes with at least 10 antisense reads per million total reads in wild-type. The levels of microRNAs and 21U–RNAs were unaffected in *rde-8(ne3361)* mutants (Figure 2A, B, and S2). The 22G-RNA defect of *rde-8(ne3361)* was strongly rescued (87% of target genes; n=1938) by *the gfp::rde-8(+)* transgene, but only partially (33.7% of target genes; n=1938) by the active-site mutant *gfp::rde-8(D76N)* transgene (Figure 2D).

Examining the levels of 22G-RNAs antisense to genes targeted by ERGO-1, WAGO, or CSR-1 (Claycomb et al., 2009; Gu et al., 2009; Vasale et al., 2010), we found that 22G-RNAs antisense to WAGO and ERGO-1 targets were reduced in *rde-8* mutants, whereas 22G-RNAs antisense to CSR-1 targets were mostly unaffected (Figure 2E and Table S1). The ERGO-1- and WAGO-dependent 22G-RNA defects were rescued by the *gfp::rde-8(+)* transgene, but not by the active-site mutant *gfp::rde-8(D76N)* transgene (Figure 2E). WAGO 22G-RNAs dependent on RDE-8 activity included 22G-RNAs that also depend on the PRG-1/piRNA pathway (Table S2; Gu et al., 2009; Lee et al., 2012). RDE-8-dependent 22G-RNAs also included RDE-1/*mir-243*-dependent 22G-RNAs that silence *y47h10a.5* in the soma (Table S1; Correa et al., 2010; Gu et al., 2009). Thus the small RNA defects of *rde-8* mutants are consistent with the RNAi and transgene silencing defects of *rde-8* mutants

and suggest that RDE-8 activity is required for the production or accumulation of RdRP-dependent siRNAs that function in the WAGO and ERI silencing pathways.

To ask if RDE-8 is required for the accumulation of ERGO-1 26G-RNAs, we cloned and deep sequenced 5′-monophosphorylated small RNAs. We found that 26G-RNAs were reduced at least 2-fold in the *rde-8(ne3361)* mutant at 98% (124/126) of ERGO-1 target mRNAs with a minimum of 10 antisense 26G-RNA reads per million total non-structural reads in wild type, and at least 10-fold at 96% (121/126) of the affected loci (Figure 2F). Interestingly, in the *gfp::rde-8(D76N)* background, 26G-RNAs were reduced by at least 2-fold at only 35% (44/126) of target genes, and at least 10-fold at only three of these targets (Figure 2F). Our data suggest that RDE-8 is required for the accumulation of two different classes of RdRP-generated small RNAs, WAGO 22G-RNAs and ERGO-1 26G-RNAs, but the ribonuclease activity of RDE-8 is not required for 26G-RNA accumulation.

RDE-8 interacts with ERI/DICER and RNAi/Mutator pathway components

To understand how RDE-8 promotes RNAi and 22G-RNA biogenesis, we sought to identify proteins that interact with RDE-8. Using size-exclusion chromatography to examine the molecular weight of RDE-8 complexes in worm lysates, we found that endogenous RDE-8, which has a molecular weight of 38.8 kDa, migrated between 158 kDa (Aldolase) and 440 kDa (Ferritin) in gel filtration analysis (Figure S3). GFP::RDE-8 did not coimmunoprecipitate (co-IP) with endogenous RDE-8 (data not shown), suggesting that the higher molecular weight complexes are not comprised of RDE-8 multimers. Using multidimensional protein identification technology (MudPIT; Chen et al., 2006), we identified several RDE-8-interacting proteins whose loss-of-function phenotypes are similar to those of *rde-8* (Figure 3A and Table S4), including the β-nucleotidyltransferase RDE-3, MUT-15/RDE-5, and the Q/N-domain protein MUT-16/RDE-6 (Chen et al., 2005; Vastenhouw et al., 2003; Gu et al., 2009; Zhang et al., 2011).

Interestingly, we found that three RDE-8 interactors are homologous to RDE-8, including ERI-9 and two previously unstudied proteins, T23G4.3 and Y87G2A.7, which we have named NYN-1 and NYN-2, respectively. ERI-9 was previously shown to be required for 26G-RNA biogenesis (Pavelec et al., 2009). Consistent with the association of RDE-8 with ERI/Dicer complex components (Duchaine et al., 2006), we found that RDE-8 also co-IPs with the SAP-domain exonuclease ERI-1b (Figure S3; Kennedy et al., 2004), which interacts with both ERI-9 and Dicer and is required for the RdRP-dependent biogenesis of 26G-RNAs (Duchaine et al., 2006; Pavelec et al., 2009; Thivierge et al., 2012).

NYN-1 and NYN-2 are paralogs and more similar to ERI-9 than to other *C. elegans* NYN-domain proteins, yet were more highly enriched than ERI-9 in RDE-8 IPs. To test whether NYN-1 and NYN-2 are required for exo-RNAi, we obtained deletion alleles of *nyn-1* (*tm5004* and *tm5149*) and *nyn-2*(*tm4844*). Single mutants were fully sensitive to RNAi in the germline (*pos-1*) and soma (*let-2*), but *nyn-1; nyn-2* double mutants were strongly RNAi deficient in both tissue types (Figure 3B). Thus, NYN-1 and NYN-2 appear to act redundantly in the exo-RNAi pathway.

Consistent with the RNAi defect of *nyn-1; nyn-2* mutants, we found that WAGO-dependent 22G-RNAs and ERI-pathway small RNAs (both 26G-RNAs and 22G-RNAs) were markedly reduced (Figure 3C, 3D and Figure S3). A triple *nyn-1; nyn-2; rde-8* mutant did not significantly enhance the 22G-RNA defect (Figure S3). Together, our findings suggest that NYN-1 and NYN-2 function with RDE-8 and transposon-silencing factors to promote the biogenesis of RdRP-dependent siRNAs in WAGO- and ERI-dependent silencing pathways.

RDE-8 localizes to P-granule-associated Mutator foci

The identification of MUT-16/RDE-6, MUT-15/RDE-5, and RDE-3/MUT-2 as RDE-8 interactors suggested that RDE-8 might localize to recently described Mutator foci: perinuclear germline foci that are distinct from, but often adjacent to, germline P-granules (Phillips et al., 2012). Indeed, endogenous RDE-8 protein was most abundant in the hermaphrodite or female germline (Figure 4A), and GFP::RDE-8 was primarily observed in the germline cytoplasm and in prominent perinuclear foci associated with nuclear pores in the germline (Figure 4B). Moreover, perinuclear GFP::RDE-8 foci were both fewer in number than and adjacent to P-granules identified by RFP::PGL-1 (Figure 4C; Wolke et al., 2007). These data are consistent with the idea that RDE-8 functions along with its interactors MUT-16, MUT-15, and RDE-3 in Mutator foci.

RDE-8 is important for efficient RdRP activity

RDE-8 is required for RdRP-dependent siRNA accumulation and interacts with several components of Mutator foci, which are thought to be compartments where RdRP activity promotes siRNA accumulation (Phillips et al., 2012). However, RDE-8 and RdRP interactions were not detected reproducibly in our co-IP studies (data not shown). To ask if RDE-8 promotes RdRP activity in vitro, we used an assay in which the de novo synthesis of 22G-RNAs is dependent on the RdRP RRF-1, the β-nucleotidyltransferase RDE-3, and a template RNA that is not polyadenylated (Figure 5; Aoki et al., 2007). Consistent with the reduced level of 22G-RNAs observed in *rde-8* mutants, we found that the activity of RdRP was reduced by ∼50% in the *rde-8(ne3361)* lysate relative to the wild-type lysate (Figure 5 and Experimental Procedures). The levels of RRF-1 protein and a control protein (PRG-1) were similar in the *rde-8(ne3361)* and wild-type lysates (Figure 5A). RdRP was also less active in a *gfp::rde-8(D76N)* lysate relative to a *gfp::rde-8(+)* lysate (Figure 5B). These findings suggest that RDE-8 is important for efficient RdRP activity.

RDE-8 interacts with target mRNA and requires RDE-1 and trigger dsRNA

To ask whether RDE-8 interacts with the target mRNA during RNAi, we immunoprecipitated GFP::RDE-8 from worms exposed to dsRNA targeting *sel-1* or a negative control, and then used RT-qPCR to detect regions of the *sel-1* mRNA (Figure 6A). We failed to detect a significant enrichment of *sel-1* mRNA in GFP::RDE-8(WT) IP experiments (Figure 6B). This lack of enrichment could result from GFP::RDE-8(WT) binding only transiently to the *sel-1* mRNA and then perhaps rapidly cleaving and releasing it. We therefore also tested for RNA binding by the catalytically inactive GFP::RDE-8(D76N). Strikingly, we found that RDE-8(D76N) specifically captured the

sel-1 transcript when animals were exposed to *sel-1* dsRNA (Figure 6A). Interestingly, GFP::RDE-8(D76N) IP enriched similar levels of *sel-1* mRNA from both upstream and downstream of the dsRNA trigger region (regions 1 and 4, Figure 6A) suggesting that GFP::RDE-8(D76N) associates with an intact *sel-1* transcript, one that has not already been cleaved by the primary Argonaute RDE-1 (see below and Discussion).

We next examined the genetic requirement for target mRNA recognition by GFP::RDE-8(D76N). The Argonaute RDE-1 is required for the initiation of RNAi and is loaded with primary siRNAs processed from dsRNA by Dicer (Yigit et al., 2006). Dicer-dependent primary siRNAs are present in *rde-8* mutants (Figure 2C), and based on affinity capture experiments using 2′-O-methylated RNA oligos, they are loaded onto functional RDE-1 complexes (Figure S4). Consistent with the idea that these primary RDE-1/siRNA complexes are required for RDE-8 to interact with the target, we found that GFP::RDE-8(D76N) failed to capture target mRNA in the *rde-1(ne300)* mutant background (Figure 6B). The ability of RDE-1 to promote RDE-8 binding to the target is likely to be independent of RDE-1 catalytic activity, since the catalytic mutant RDE-1(AAA) protein promotes secondary siRNA biogenesis and silencing triggered by dsRNA (Pak et al., 2012; Steiner et al., 2009). As expected, we found that the ability of RDE-1(AAA) to promote *sel-1(RNAi)* is dependent on RDE-8 catalytic activity. *sel-1(RNAi)* dramatically reduced *sel-1* mRNA levels in *rde-1(AAA)* animals, but not in *rde-1(AAA); gfp::rde-8(D76N)* animals (Figure S4). Thus, RDE-8 functions downstream of target recognition by RDE-1.

We next asked whether RdRP is required for RDE-8 to bind target mRNA. To remove RdRP activity it was necessary to use the double mutant *rrf-1(pk1417) glp-4(bn2)* background, in which the somatic RdRP *rrf-1* is deleted and the germline RdRP *ego-1* (Smardon et al., 2000) is not expressed due to the absence of germline at 25°C in the temperature-sensitive, germline-deficient mutant *glp-4(bn2)* (Beanan and Strome, 1992). Conditional alleles of *ego-1*, which is an essential gene, do not exist. We found that depletion of RdRP failed to block the association of GFP::RDE-8(D76N) with *sel-1* target mRNA (Figure 6B). Thus RDE-8 recognizes the target transcript upstream of RdRP and secondary small RNA amplification.

Finally, we asked whether RDE-8 interactors are required for RDE-8 to bind the target. In *mut-15(tm1358)*, *mut-16(tm3748)*, or *nyn-1(tm5004); nyn-2(tm4844)* mutants, enrichment of *sel-1* mRNA by GFP::RDE-8(D76N) RIP was reduced to 22–42% of the WT level (Figure 6B). By contrast, we found that GFP::RDE-8(D76N) RIP in the *rde-3(ne3370)* mutant background enriched *sel-1* mRNA to 77% of WT levels (Figure 6B). These data suggest that RDE-8 interactors facilitate or stabilize RDE-8 binding to the target mRNA and function together upstream of RdRP. The β-nucleotidyltransferase RDE-3, however, appears to be less important for RDE-8 binding to the target than for RdRP activity, suggesting that RDE-3 may function between RDE-8 and RdRP.

RDE-8 is required for the accumulation of 3′ uridylated mRNA cleavage products

Upstream components of the *C. elegans* RNAi machinery must somehow generate mRNA-derived templates for the RdRP-dependent amplification of the silencing signal. In *Tetrahymena*, efficient RdRP recruitment requires 3′ uridylation of RNA templates (Lee et

al., 2009; Talsky and Collins, 2010). We therefore asked if target mRNA fragments tailed with untemplated residues accumulate during RNAi in *C. elegans* and, if so, whether or not these products are dependent on RDE-8 activity. To do this, we used 3′ rapid amplification of cDNA ends (RACE) to search for mRNA cleavage products in animals exposed to dsRNA targeting the *sel-1* transcript and in control animals not exposed to dsRNA. A 3′ linker was ligated to the RNA to provide an anchor for first-strand cDNA synthesis and subsequent PCR reactions. To amplify potential 3′ *sel-1* mRNA cleavage products, and not the ingested *sel-1* dsRNA, we amplified each cDNA library using a series of nested *sel-1* mRNA-specific primers to generate 3′ RACE products with 5’ ends that lie 40, 30, 20, and 12 nts upstream of the dsRNA target sequence. The nested cDNAs were pooled and amplified, and 3′ RACE products were gel purified and deep sequenced (Figure S5).

Consistent with the idea that RDE-8 activity is important for target cleavage, we found that target-mRNA fragments tended to be higher in *gfp::rde-8(+)* worms than in *gfp::rde-8(D76N)* worms after 3 and 7 hours of RNAi (Figure S6). Notably, we found that target-mRNA fragments containing untemplated uridines (but not untemplated A, C, or G residues) increased in *gfp::rde-8(+)* rescued *rde-8(ne3361)* animals exposed to RNAi by 5.5-fold after 3 hours and by 20-fold after 7 hours (Figure 7A). These time points correspond to the interval where 22G-RNA production is first detectable during RNAi (Figures 2C, 7B). By contrast, the levels of uridylated *sel-1* fragments remained low in *rde-8(ne3361); gfp::rde-8(D76N)* transgenic worms throughout the *sel-1(RNAi)* time course and in *gfp::rde-8(+)* rescued animals that were not exposed to *sel-1* dsRNA (Figure 7A–C). In wild-type worms expressing endogenous RDE-8, we found that fragments modified with 2 untemplated uridine residues were the most prominent species after 3 hours *of sel-1(RNAi)*, but fragments with 1, 2, 3, or 4 untemplated uridines were observed at similar levels after 7 hours (Figure 7B). In the *gfp::rde-8(+)* strain, however, mono-uridylated fragments were by far the most prominent species (Figure 7B).

To examine the possible relationship between 3′ uridylation and RdRP function, we cloned and deep sequenced 22G-RNAs from each time point in the *gfp::rde-8(+)* and *gfp::rde-8(D76N)* transgenic strains. When we mapped the 3′ uridylation and 22G-RNA initiation sites, we observed at least one 22G-RNA peak that initiates 5′ and proximal to the major uridylation sites in *gfp::rde-8(WT)*, but not *gfp::rde-8(D76N)*, transgenic worms (Figure 7B). In addition, the 3′ uridylation products were observed at 3 h, whereas the corresponding 22G-RNAs were not detected until 7 h, suggesting that the accumulation of uridylated *sel-1* fragments precedes the accumulation of the corresponding 22G-RNAs at these sites.

Finally, we examined whether the accumulation of uridylated target mRNA fragments depends on RdRP and RDE-3 activity. Depleting RdRP activity, using an *rrf-1(pk1417) glp-4(bn2)* double mutant background as described above, we found that *sel-1* mRNA fragments were uridylated proximal to the dsRNA trigger region in *rde-8(ne3361); gfp::rde-8(+)* animals, but uridylation was reduced in *rde-8(ne3361); gfp::rde-8(D76N)* animals and in *rde-3(ne3370)* animals (Figure 7D). In these experiments, the pattern of uridylation differed from that observed in the time course above (perhaps owing to the lack of germline or RdRP). These data suggest that, together, RDE-8 and RDE-3 act upstream of

RdRP to promote the uridylation of 5′ *sel-1* fragments that could function as RdRP templates.

DISCUSSION

The RdRP-dependent amplification of secondary siRNAs is essential for robust silencing during RNAi in *C. elegans*. Thus target mRNA destruction must be managed during RNAi so as to preserve mRNA sequences that serve as templates for RdRP amplification. In this study, we have shown that RDE-8 encodes a ribonuclease that interacts with target mRNA downstream of the Argonaute RDE-1 but upstream of RDE-3 and RdRP. RDE-8 forms a complex with RDE-3 in vivo and is required for the uridylation of 5′ fragments of the target mRNA and for the amplification of secondary siRNAs by RdRP.

It is well known that a number of viral RdRPs prefer to initiate de novo transcription using GTP (Kao et al., 2001). Furthermore, the *Neurospora* RdRP QDE-1, a homolog of worm RdRPs, prefers to initiate de novo transcription with GTP and to produce 9- to 21-nt small RNAs that are distributed across the template (Makeyev and Bamford, 2002). In *C. elegans*, RdRPs prefer to initiate transcription at a YG motif (as viewed from the antisense strand), where G is the 1st nucleotide of the 22G-RNA preceded by a pyrimidine (Y), which is similar to the YR motif preferred by RNA polymerase II for transcription initiation, where a purine (R) is the 1st nucleotide of the transcript (Gu et al., 2012, and references therein).

Our findings suggest a model (Figure 7E) whereby mRNAs are initially recognized but not cleaved by RDE-1. Instead, RDE-1 recruits a complex containing RDE-8, which cleaves the target mRNA exposing a 3′ end that can be uridylated by the P-nucleotidyltransferase homolog RDE-3. Thus RDE-8 cleavage and RDE-3-dependent 3′ uridylation of cleavage products may provide a signal or platform to recruit the RdRP complex. RdRP could then, in turn, initiate de novo transcription from internal C nucleotides near the 3′ end of the uridylated template. This model is consistent with previous work showing that 22G-RNA amplification is highest proximal to the dsRNA trigger region (Sijen et al., 2001; Sijen et al., 2007; Pak and Fire, 2007). RDE-8 may function similarly in the ERI pathway, after ERGO-1 targeting, and may also function along with RDE-3 downstream of WAGO-mediated target recognition.

The nuclease activity of recombinant RDE-8 requires conserved aspartic acid residues that map to the catalytic site of Zc3h12a (Matsushita et al., 2009; Xu et al., 2012). Zc3h12a destabilizes the mRNAs of immune-related factors, including IL-6 and IL-12p40, by directly binding and cleaving 3′ UTRs (Matsushita et al., 2009). Zc3h12a was also shown to negatively regulate miRNA expression by cleaving the terminal loop of pre-miRNAs (Suzuki et al., 2011). The CCCH domain of Zc3h12a is required for RNA-binding activity in vitro and for cleavage in vivo but not in vitro (Suzuki et al., 2011). RDE-8 contains no recognizable RNA-binding domain, and we only detected target binding when the conserved catalytic residues of RDE-8 were mutated, suggesting a transient or indirect interaction between RDE-8 and the target mRNA. Perhaps consistent with the latter possibility, the interaction with target mRNA was partially dependent on factors that interact with RDE-8

and required the Argonaute RDE-1, which may directly or indirectly recruit the RDE-8 complex to the target mRNA.

Among the factors that interact with RDE-8, we identified three homologs of RDE-8, including ERI-9 and the closely related redundant genes NYN-1 and NYN-2. Previous work has shown that ERI-9 is a component of the ERI complex and is required for ERI endo-siRNAs expressed in embryos (Duchaine et al., 2006; Pavelec et al., 2009). Our small RNA data indicate that RDE-8, NYN-1, and NYN-2 function along with ERI-9 in the ERI pathway. Remarkably, ERI-9, NYN-1, and NYN-2 lack predicted active-site residues and are thus unlikely to encode functional nucleases. Nevertheless, these factors were required for ERI-pathway 26G-RNA and 22G-RNA biogenesis, and NYN-1 and NYN-2 were also required for RDE-8(D76N) to interact with the target mRNA during RNAi and for RDE-8 to localize to Mutator foci. Together, these results suggest a structural rather than catalytic role for ERI-9, NYN-1, and NYN-2 in the RDE-8 complex. Interestingly, although the catalytic activity of RDE-8 was required for 22G-RNA biogenesis, it was not required for 26G-RNA accumulation. Perhaps RDE-8 and ERI-9 are structurally important for a functional ERI complex, promoting RRF-3–dependent 26G-RNA biogenesis. A structural role for ribonucleases is well documented; the eukaryotic PM/Scl complex, or exosome, for example, is composed of multiple RNasePH family members that lack catalytic capacity (Jain, 2012). Detailed structure-function studies are necessary to sort out the role of these and six other RDE-8 homologs in *C. elegans*. Our findings along with previous work on Zc3h12a suggest that members of this conserved nuclease family share ancient and fundamental roles in immunity.

How does RDE-8 function during RNAi?

Several studies suggest that direct Argonaute-mediated target mRNA cleavage is not required for mRNA silencing during RNAi (and related pathways) in *C. elegans*. For example, when engineered to contain mutations in conserved metal-coordinating residues needed by other Argonautes for RNA cleavage, RDE-1 and PRG-1 could nevertheless initiate RdRP recruitment and gene silencing in the dsRNA- and piRNA-initated pathways, respectively (Bagijn et al., 2012; Lee et al., 2012; Pak and Fire, 2007; Shirayama et al., 2012; Steiner et al., 2009). Moreover, all twelve of the downstream WAGO Argonautes, required for silencing in both of these pathways, encode proteins that lack key residues required for target cleavage (Yigit et al., 2006). Similarly, *Rhodobacter sphaeroides* Argonaute is not a functional endonuclease, but promotes the silencing of foreign genetic material (Olovnikov et al., 2013). These observations suggest that, in the absence of endonuclease activity, Argonautes can promote silencing by guiding other nucleases or turnover pathways to their targets (Huntzinger and Izaurralde, 2011; Lim et al., 2014). Our finding that target mRNA cleavage products with untemplated uridine residues accumulate during RNAi in an RDE-8-dependent manner raises the possibility that RDE-8 (or other components of the RDE-8 complex) may provide cleavage activity important for RNAi. Our findings place RDE-8 downstream of primary Argonautes (RDE-1, ERGO-1, and PRG-1) and upstream or at the same level as RdRP in each of these pathways.

Several recent studies have identified factors that appear to function between RDE-1 and RdRP, including RDE-10, RDE-11, and RDE-12 (Shirayama et al., 2014; Yang et al., 2014; Yang et al., 2012; Zhang et al., 2011). Based on IP experiments presented here and in the aforementioned studies, RDE-8 does not interact with these factors. Furthermore, RDE-10, RDE-11, and RDE-12 are specifically required for WAGO-associated 22G-RNAs dependent on RDE-1 and ERGO-1 (Shirayama et al., 2014; Yang et al., 2014; Yang et al., 2012; Zhang et al., 2011), whereas RDE-8 is more broadly required for WAGO-associated 22G-RNAs. Thus, RDE-8 may function at a distinct step (or multiple steps) in the RNAi pathway.

Finally, RDE-8 also promotes the accumulation of WAGO-associated 22G-RNAs that are independent of known primary Argonautes and thus appear to function in self-enforcing trans-generational silencing pathways. It is tempting to speculate that WAGOs have evolved catalytic mutations so that they do not cleave the target mRNA within the region required to template de novo synthesis of the siRNAs that successfully guided them to the target. Instead, WAGOs may recruit secondary nucleases that cleave the target mRNA 3′ of where their guide RNAs engage the target. The β-nucleotidyltransferase homolog RDE-3 could then modify this cleavage product to stabilize it or to recruit RdRP to regenerate the 22G-RNA, thereby propagating self-enforcing silencing signals (Figure 7E). In contrast, perhaps RDE-1 recruits RDE-8 more broadly along the target mRNA producing multiple cleavage products that can serve to generate new RdRP derived siRNAs (Figure 7E).

Conclusion

RDE-8 homologs regulate post-transcriptional silencing in innate immune pathways in both worms and mammals. Our findings suggest that RDE-8 homologs might function as nucleases or as structural subunits of silencing complexes that promote 3′ uridylation of substrates. Uridylation plays diverse and important roles in small RNA pathways (Lee et al., 2014; Talsky and Collins, 2010). In plants and animals, 3′ uridylation promotes the turnover of miRNAs and siRNAs (Ameres et al., 2010; Ibrahim et al., 2010), and miRNA- or siRNA-directed cleavage of mRNA results in 3′ uridylation of the 5′ cleavage product and rapid mRNA decay (Shen and Goodman, 2004). Moreover, Kim and colleagues have recently shown that 3′ uridylation enhances mRNA decay of deadenylated miRNA targets (Lim et al., 2014). Perhaps 3′ uridylation of transcripts processed by RDE-8-related nucleases is a conserved signal for post-transcriptional silencing. It will therefore be interesting to learn whether RDE-8-related proteins function broadly in uridylation-dependent pathways that regulate gene expression.

EXPERIMENTAL PROCEDURES

Genetics

C. elegans culture and genetics were performed essentially as described (Brenner, 1974). Unless otherwise noted, the wild-type (WT) strain in this study is the Bristol N2 strain. Alleles used in this study listed by chromosome: LGI: *mut-16(tm3748, ne322)*, *rde-3(ne3370)*, *rrf-1(pk1417)*, *glp-4 (bn2)*, *nyn-2(tm4844)*; LGII: *neSi24[gfp::rde-8(+), cb-unc-119(+)]*, *neSi25[gfp::rde-8(D76N), cb-unc-119(+)]*; LGIV: *rde-8(ne3361, tm2192, tm2252)*, *fem-1(hc17)*, *nyn-1(tm5004, tm5149)*; LGV: *rde-1(ne300)*, *mut-15(tm1358)*, *fog-2*

(q71). The genetic screen and transgenic procedures are detailed in Extended Experimental Procedures.

Recombinant RDE-8 protein purification and ribonuclease assay

rde-8 cDNAs (wild-type and D76N) were cloned into a pET expression vector. Expression was induced in BL21(DE3) cells at 16°C overnight. 6His-RDE-8 fusion proteins were extracted in 50mM Tris pH 7.5, 50mM NaCl by sonication. Soluble 6His-RDE-8 fusion proteins were purified by anion exchange (Q-Sepharose), nickel-chelate, and gel-filtration chromatography. Proteins purity was verified by SDS-PAGE. Nuclease assays were performed as described in Matsushita et al. (2009), but the buffer was adjusted to pH 6.0.

RNA immunoprecipitation

Worms were harvested as adults and extracted in 1 pellet volume of homogenization buffer [25 mM Hepes-KOH ph7.5, 10 mM potassium acetate, 2 mM magnesium chloride, 0.1% NP-40, 110 mM potassium chloride, 200U/ml SUPERaseIn (Ambion)]. 20 mg of lysate was incubated with 20 μg of anti-GFP antibody (Wako) or IgG control for 1 hr at 4°C. Immune complexes were captured with Protein A/G-Sepharose beads (Santa Cruz Biotechnology) and washed with homogenization buffer. RNA was extracted with Trizol (MRC, Inc) and cDNA was prepared using SuperScript III (Life Technologies) and a mixture of *sel-1* and *act-3* primers. The level of *sel-1* mRNA was measured by quantitative PCR relative to *act-3*. Primers are listed in Extended Experimental Procedures.

MudPIT

MudPIT analysis was performed essentially as described (Conine et al., 2013). See Extended Experimental Procedures for details.

Small RNA cloning and data analysis

Small RNAs between 18 and 40 nt were gel purified and cloned after treatment with CIP (NEB) and PNK (NEB), or without pretreatment (direct cloning), as described (Gu et al., 2009; Vasale et al., 2010). Libraries were sequenced either on an Illumina GAII or HiSeq instrument in the UMass Medical School Deep Sequencing Core. Sequences were aligned to the worm genome (WS235) using Bowtie 0.12.9 (Langmead et al., 2009). Custom Python scripts used to process and analyze the data are available upon request. See Extended Experimental Procedures for details.

3′ RACE sequencing

Total RNA was extracted from worms fed with bacteria expressing *sel-1* or control dsRNA. RNAs were ligated to the activated 3′ linker, miR Linker 1 (IDT). Ligation products were reverse transcribed using a primer specific to the 3′ linker sequence. Libraries were generated by nested PCR and sequenced on an Illumina HiSeq 2000 instrument. See Extended Experimental Procedures for details.

RdRP assay

The in vitro RdRP assay (Aoki et al., 2008) was performed 4 times. Lysates were prepared from synchronized adult worms. Labeled products separated on a 15% polyacrylamide/8 M urea gel were detected and quantified using a Storm phosphorimager and ImageQuant software (GE Healthcare). The rate of ^{32}P-UTP incorporation into siRNAs by RdRP was calculated as the slope of time-course data (e.g., Figure 5) fitted to a linear function.

Fluorescence imaging

Gonads of adult *rde-8(ne3361); gfp::rde-8(+)* animals were extruded by decapitating worms on a slide. Extruded gonads were fixed with formaldehyde, permeabilized by freeze-cracking, and stained as described (Phillips et al., 2009). Confocal images were acquired using a Zeiss LSM510 Meta Confocal microscope and Zen 2008 (Zeiss) software.

Supplementary Material

Refer to Web version on PubMed Central for supplementary material.

ACKNOWLEDGEMENTS

We thank members of the Mello lab for great discussion; E. Kittler and the UMass Deep Sequencing Core for Illumina sequencing; P. Furcinitti and the UMass Light Microscopy Core and the Academia Sinica, Institute of Biological Chemistry Imaging & Cell Biology Core facilities for help with confocal microscopy. Some strains were provided by the *Caenorhabditis* Genetics Center, which is funded by NIH Office of Research Infrastructure Programs (P40 OD010440). H.Y.T was supported by a fellowship from the Leukemia and Lymphoma Society (5247-09). J.J.M. and J.R.Y. were supported by the National Center for Research Resources (5P41RR011823), National Institute on Aging (R01AG027463), and National Institute of General Medical Sciences (8P41GM103533). D.A.C. is supported by Fundação para Ciência e a Tecnologia, Portugal (SFRH/BD/17629/2004/H6BM). M.D.T. is supported by Academia Sinica. C.C.M. is a Howard Hughes Medical Institute Investigator and is supported by NIH grants GM058800 and 1S10RR027052

REFERENCES

Ameres SL, Horwich MD, Hung JH, Xu J, Ghildiyal M, Weng Z, Zamore PD. Target RNA-directed trimming and tailing of small silencing RNAs. Science. 2010; 328:1534–1539. [PubMed: 20558712]

Anantharaman V, Aravind L. The NYN domains: novel predicted RNAses with a PIN domain-like fold. RNA Biol. 2006; 3:18–27. [PubMed: 17114934]

Aoki K, Moriguchi H, Yoshioka T, Okawa K, Tabara H. In vitro analyses of the production and activity of secondary small interfering RNAs in C. elegans. EMBO J. 2007; 26:5007–5019. [PubMed: 18007599]

Ashe A, Sapetschnig A, Weick EM, Mitchell J, Bagijn MP, Cording AC, Doebley AL, Goldstein LD, Lehrbach NJ, Le Pen J, et al. piRNAs can trigger a multigenerational epigenetic memory in the germline of C. elegans. Cell. 2012; 150:88–99. [PubMed: 22738725]

Bagijn MP, Goldstein LD, Sapetschnig A, Weick EM, Bouasker S, Lehrbach NJ, Simard MJ, Miska EA. Function, targets, and evolution of Caenorhabditis elegans piRNAs. Science. 2012; 337:574–578. [PubMed: 22700655]

Batista PJ, Ruby JG, Claycomb JM, Chiang R, Fahlgren N, Kasschau KD, Chaves DA, Gu W, Vasale JJ, Duan S, et al. PRG-1 and 21U–RNAs interact to form the piRNA complex required for fertility in C. elegans. Mol. Cell. 2008; 31:67–78. [PubMed: 18571452]

Beanan MJ, Strome S. Characterization of a germ-line proliferation mutation in C. elegans. Development. 1992; 116:755–766. [PubMed: 1289064]

Brenner S. The genetics of Caenorhabditis elegans. Genetics. 1974; 77:71–94. [PubMed: 4366476]

Buckley BA, Burkhart KB, Gu SG, Spracklin G, Kershner A, Fritz H, Kimble J, Fire A, Kennedy S. A nuclear Argonaute promotes multigenerational epigenetic inheritance and germline immortality. Nature. 2012; 489:447–451. [PubMed: 22810588]

Castel SE, Martienssen RA. RNA interference in the nucleus: roles for small RNAs in transcription, epigenetics and beyond. Nat. Rev. Genet. 2013; 14:100–112. [PubMed: 23329111]

Chen CC, Simard MJ, Tabara H, Brownell DR, McCollough JA, Mello CC. A member of the polymerase beta nucleotidyltransferase superfamily is required for RNA interference in C. elegans. Curr. Biol. 2005; 15:378–383. [PubMed: 15723801]

Chen EI, Hewel J, Felding-Habermann B, Yates JR 3rd. Large scale protein profiling by combination of protein fractionation and multidimensional protein identification technology (MudPIT). Mol. Cell. Proteomics. 2006; 5:53–56. [PubMed: 16272560]

Claycomb JM, Batista PJ, Pang KM, Gu W, Vasale JJ, van Wolfswinkel JC, Chaves DA, Shirayama M, Mitani S, Ketting RF, et al. The Argonaute CSR-1 and its 22G-RNA cofactors are required for holocentric chromosome segregation. Cell. 2009; 139:123–134. [PubMed: 19804758]

Conine CC, Moresco JJ, Gu W, Shirayama M, Conte D Jr, Yates JR 3rd, Mello CC. Argonautes promote male fertility and provide a paternal memory of germline gene expression in C. elegans. Cell. 2013; 155:1532–1544. [PubMed: 24360276]

Correa RL, Steiner FA, Berezikov E, Ketting RF. MicroRNA-directed siRNA biogenesis in Caenorhabditis elegans. PLoS Genet. 2010; 6:e1000903. [PubMed: 20386745]

Das PP, Bagijn MP, Goldstein LD, Woolford JR, Lehrbach NJ, Sapetschnig A, Buhecha HR, Gilchrist MJ, Howe KL, Stark R, et al. Piwi and piRNAs act upstream of an endogenous siRNA pathway to suppress Tc3 transposon mobility in the Caenorhabditis elegans germline. Mol. Cell. 2008; 31:79–90. [PubMed: 18571451]

Duchaine TF, Wohlschlegel JA, Kennedy S, Bei Y, Conte D Jr, Pang K, Brownell DR, Harding S, Mitani S, Ruvkun G, et al. Functional proteomics reveals the biochemical niche of C. elegans DCR-1 in multiple small-RNA-mediated pathways. Cell. 2006; 124:343–354. [PubMed: 16439208]

Gent JI, Lamm AT, Pavelec DM, Maniar JM, Parameswaran P, Tao L, Kennedy S, Fire AZ. Distinct phases of siRNA synthesis in an endogenous RNAi pathway in C. elegans soma. Mol. Cell. 2010; 37:679–689. [PubMed: 20116306]

Ghildiyal M, Zamore PD. Small silencing RNAs: an expanding universe. Nat. Rev. Genet. 2009; 10:94–108. [PubMed: 19148191]

Gu W, Shirayama M, Conte D Jr, Vasale J, Batista PJ, Claycomb JM, Moresco JJ, Youngman EM, Keys J, Stoltz MJ, et al. Distinct argonaute-mediated 22G-RNA pathways direct genome surveillance in the C. elegans germline. Mol. Cell. 2009; 36:231–244. [PubMed: 19800275]

Guang S, Bochner AF, Burkhart KB, Burton N, Pavelec DM, Kennedy S. Small regulatory RNAs inhibit RNA polymerase II during the elongation phase of transcription. Nature. 2010; 465:1097–1101. [PubMed: 20543824]

Guang S, Bochner AF, Pavelec DM, Burkhart KB, Harding S, Lachowiec J, Kennedy S. An Argonaute transports siRNAs from the cytoplasm to the nucleus. Science. 2008; 321:537–541. [PubMed: 18653886]

Huntzinger E, Izaurralde E. Gene silencing by microRNAs: contributions of translational repression and mRNA decay. Nat. Rev. Genet. 2011; 12:99–110. [PubMed: 21245828]

Ibrahim F, Rymarquis LA, Kim EJ, Becker J, Balassa E, Green PJ, Cerutti H. Uridylation of mature miRNAs and siRNAs by the MUT68 nucleotidyltransferase promotes their degradation in Chlamydomonas. Proc. Natl. Acad. Sci. USA. 2010; 107:3906–3911. [PubMed: 20142471]

Jain C. Novel role for RNase PH in the degradation of structured RNA. J. Bacteriol. 2012; 194:3883–3890. [PubMed: 22609921]

Kao CC, Singh P, Ecker DJ. De novo initiation of viral RNA-dependent RNA synthesis. Virology. 2001; 287:251–260. [PubMed: 11531403]

Kennedy S, Wang D, Ruvkun G. A conserved siRNA-degrading RNase negatively regulates RNA interference in C. elegans. Nature. 2004; 427:645–649. [PubMed: 14961122]

Langmead B, Trapnell C, Pop M, Salzberg SL. Ultrafast and memory-efficient alignment of short DNA sequences to the human genome. Genome Biol. 2009; 10:R25. [PubMed: 19261174]

Lee HC, Gu W, Shirayama M, Youngman E, Conte D Jr, Mello CC. C. elegans piRNAs mediate the genome-wide surveillance of germline transcripts. Cell. 2012; 150:78–87. [PubMed: 22738724]

Lee M, Kim B, Kim VN. Emerging roles of RNA modification: m(6)A and U-tail. Cell. 2014; 158:980–987. [PubMed: 25171402]

Lee SR, Talsky KB, Collins K. A single RNA-dependent RNA polymerase assembles with mutually exclusive nucleotidyl transferase subunits to direct different pathways of small RNA biogenesis. RNA. 2009; 15:1363–1374. [PubMed: 19451546]

Lim J, Ha M, Chang H, Kwon SC, Simanshu DK, Patel DJ, Kim VN. Uridylation by TUT4 and TUT7 marks mRNA for degradation. Cell. 2014; 159:1365–1376. [PubMed: 25480299]

Makeyev EV, Bamford DH. Cellular RNA-dependent RNA polymerase involved in posttranscriptional gene silencing has two distinct activity modes. Mol. Cell. 2002; 10:1417–1427. [PubMed: 12504016]

Matsushita K, Takeuchi O, Standley DM, Kumagai Y, Kawagoe T, Miyake T, Satoh T, Kato H, Tsujimura T, Nakamura H, et al. Zc3h12a is an RNase essential for controlling immune responses by regulating mRNA decay. Nature. 2009; 458:1185–1190. [PubMed: 19322177]

Olovnikov I, Chan K, Sachidanandam R, Newman DK, Aravin AA. Bacterial argonaute samples the transcriptome to identify foreign DNA. Mol. Cell. 2013; 51:594–605. [PubMed: 24034694]

Pak J, Fire A. Distinct populations of primary and secondary effectors during RNAi in C. elegans. Science. 2007; 315:241–244. [PubMed: 17124291]

Pak J, Maniar JM, Mello CC, Fire A. Protection from feed-forward amplification in an amplified RNAi mechanism. Cell. 2012; 151:885–899. [PubMed: 23141544]

Pavelec DM, Lachowiec J, Duchaine TF, Smith HE, Kennedy S. Requirement for the ERI/DICER complex in endogenous RNA interference and sperm development in Caenorhabditis elegans. Genetics. 2009; 183:1283–1295. [PubMed: 19797044]

Phillips CM, McDonald KL, Dernburg AF. Cytological analysis of meiosis in Caenorhabditis elegans. Methods Mol. Biol. 2009; 558:171–195. [PubMed: 19685325]

Phillips CM, Montgomery TA, Breen PC, Ruvkun G. MUT-16 promotes formation of perinuclear mutator foci required for RNA silencing in the C. elegans germline. Genes Dev. 2012; 26:1433–1444. [PubMed: 22713602]

Ruby JG, Jan C, Player C, Axtell MJ, Lee W, Nusbaum C, Ge H, Bartel DP. Large-scale sequencing reveals 21U–RNAs and additional microRNAs and endogenous siRNAs in C. elegans. Cell. 2006; 127:1193–1207. [PubMed: 17174894]

Seth M, Shirayama M, Gu W, Ishidate T, Conte D Jr, Mello CC. The C. elegans CSR-1 argonaute pathway counteracts epigenetic silencing to promote germline gene expression. Dev. Cell. 2013; 27:656–663. [PubMed: 24360782]

Shen B, Goodman HM. Uridine addition after microRNA-directed cleavage. Science. 2004; 306:997. [PubMed: 15528436]

Shirayama M, Seth M, Lee HC, Gu W, Ishidate T, Conte D Jr, Mello CC. piRNAs initiate an epigenetic memory of nonself RNA in the C. elegans germline. Cell. 2012; 150:65–77. [PubMed: 22738726]

Shirayama M, Stanney W 3rd, Gu W, Seth M, Mello CC. The Vasa Homolog RDE-12 engages target mRNA and multiple argonaute proteins to promote RNAi in C. elegans. Curr. Biol. 2014; 24:845–851. [PubMed: 24684931]

Sijen T, Fleenor J, Simmer F, Thijssen KL, Parrish S, Timmons L, Plasterk RH, Fire A. On the role of RNA amplification in dsRNA-triggered gene silencing. Cell. 2001; 107:465–476. [PubMed: 11719187]

Sijen T, Steiner FA, Thijssen KL, Plasterk RH. Secondary siRNAs result from unprimed RNA synthesis and form a distinct class. Science. 2007; 315:244–247. [PubMed: 17158288]

Smardon A, Spoerke JM, Stacey SC, Klein ME, Mackin N, Maine EM. EGO-1 is related to RNA-directed RNA polymerase and functions in germ-line development and RNA interference in C. elegans. Curr. Biol. 2000; 10:169–178. [PubMed: 10704412]

Steiner FA, Okihara KL, Hoogstrate SW, Sijen T, Ketting RF. RDE-1 slicer activity is required only for passenger-strand cleavage during RNAi in Caenorhabditis elegans. Nat. Struct. Mol. Biol. 2009; 16:207–211. [PubMed: 19151723]

Suzuki HI, Arase M, Matsuyama H, Choi YL, Ueno T, Mano H, Sugimoto K, Miyazono K. MCPIP1 ribonuclease antagonizes dicer and terminates microRNA biogenesis through precursor microRNA degradation. Mol. Cell. 2011; 44:424–436. [PubMed: 22055188]

Talsky KB, Collins K. Initiation by a eukaryotic RNA-dependent RNA polymerase requires looping of the template end and is influenced by the template-tailing activity of an associated uridyltransferase. J. Biol. Chem. 2010; 285:27614–27623. [PubMed: 20622019]

Thivierge C, Makil N, Flamand M, Vasale JJ, Mello CC, Wohlschlegel J, Conte D Jr, Duchaine TF. Tudor domain ERI-5 tethers an RNA-dependent RNA polymerase to DCR-1 to potentiate endo-RNAi. Nat. Struct. Mol. Biol. 2012; 19:90–97. [PubMed: 22179787]

Vasale JJ, Gu W, Thivierge C, Batista PJ, Claycomb JM, Youngman EM, Duchaine TF, Mello CC, Conte D Jr. Sequential rounds of RNA-dependent RNA transcription drive endogenous small-RNA biogenesis in the ERGO-1/Argonaute pathway. Proc. Natl. Acad. Sci. USA. 2010; 107:3582–3587. [PubMed: 20133583]

Vastenhouw NL, Fischer SE, Robert VJ, Thijssen KL, Fraser AG, Kamath RS, Ahringer J, Plasterk RH. A genome-wide screen identifies 27 genes involved in transposon silencing in C. elegans. Curr. Biol. 2003; 13:1311–1316. [PubMed: 12906791]

Wolke U, Jezuit EA, Priess JR. Actin-dependent cytoplasmic streaming in C. elegans oogenesis. Development. 2007; 134:2227–2236. [PubMed: 17507392]

Xu J, Peng W, Sun Y, Wang X, Xu Y, Li X, Gao G, Rao Z. Structural study of MCPIP1 N-terminal conserved domain reveals a PIN-like RNase. Nucleic Acids Res. 2012; 40:6957–6965. [PubMed: 22561375]

Yang H, Vallandingham J, Shiu P, Li H, Hunter CP, Mak HY. The DEAD box helicase RDE-12 promotes amplification of RNAi in cytoplasmic foci in C. elegans. Curr. Biol. 2014; 24:832–838. [PubMed: 24684930]

Yang H, Zhang Y, Vallandingham J, Li H, Florens L, Mak HY. The RDE-10/RDE-11 complex triggers RNAi-induced mRNA degradation by association with target mRNA in C. elegans. Genes Dev. 2012; 26:846–856. [PubMed: 22508728]

Yigit E, Batista PJ, Bei Y, Pang KM, Chen CC, Tolia NH, Joshua-Tor L, Mitani S, Simard MJ, Mello CC. Analysis of the C. elegans Argonaute family reveals that distinct Argonautes act sequentially during RNAi. Cell. 2006; 127:747–757. [PubMed: 17110334]

Zhang C, Montgomery TA, Gabel HW, Fischer SE, Phillips CM, Fahlgren N, Sullivan CM, Carrington JC, Ruvkun G. mut-16 and other mutator class genes modulate 22G and 26G siRNA pathways in Caenorhabditis elegans. Proc. Natl. Acad. Sci. USA. 2011; 108:1201–1208. [PubMed: 21245313]

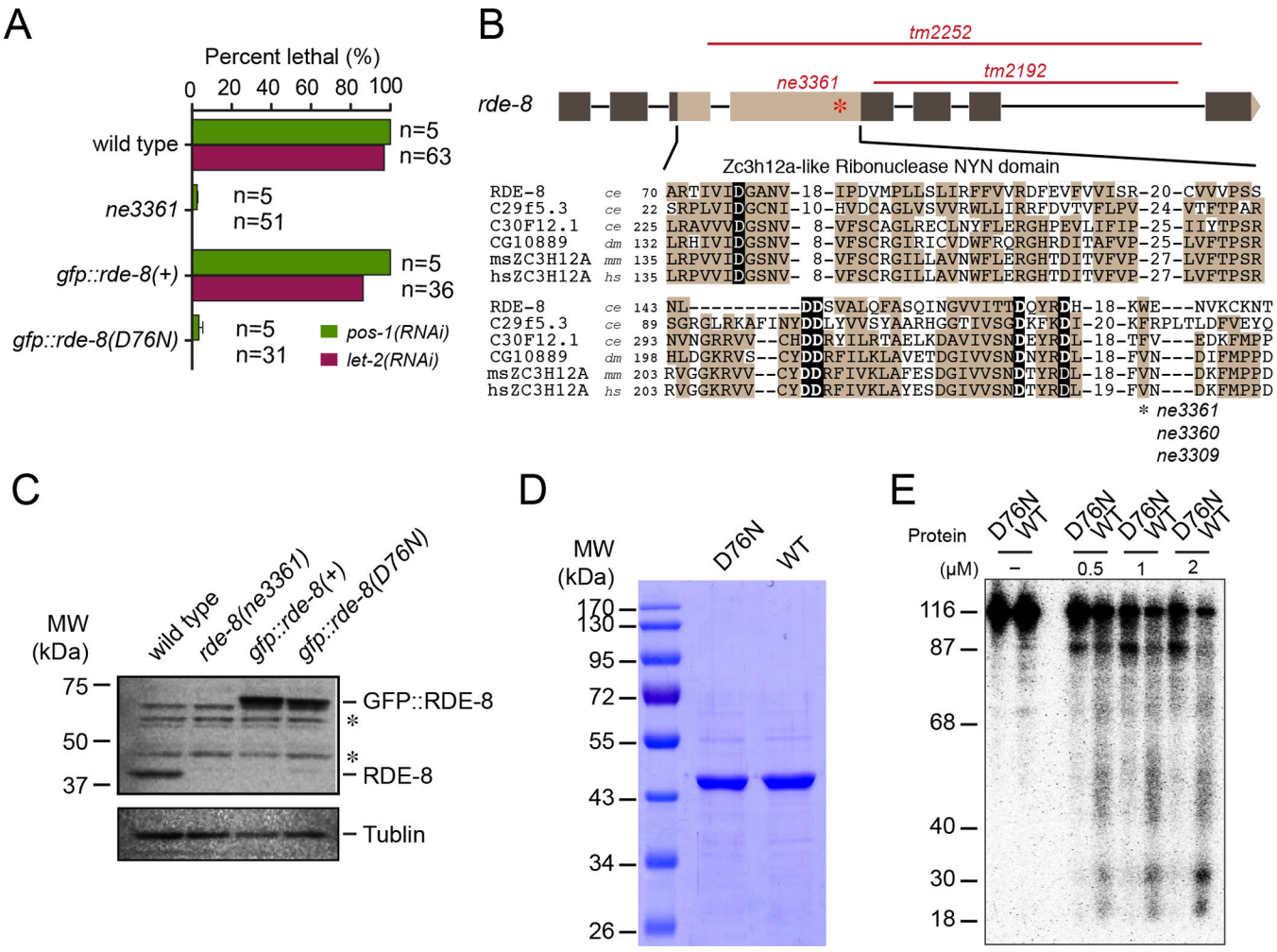

Figure 1. *rde-8* encodes a conserved ribonuclease required for RNAi

(A) Graphical representation of RNAi sensitivity in wild-type, *rde-8(ne3361)* and transgenic strains (as indicated). Percent lethal indicates the mean percentage of *pos-1* dead eggs (green bars) or the percentage of *let-2* ruptured or sterile adults observed (red bars). n, number of animals exposed to RNAi.

(B) Schematic of the *rde-8* locus showing exons (boxes) and intron (lines) with the ribonuclease domain shaded light brown. Deletion (red lines) and nonsense (asterisk) alleles are indicated. The alignment shows *C. elegans (ce)*, *Drosophila (dm)*, mouse *(mm)*, and human *(hs)* homologs with conserved residues (shaded brown) and catalytic residues (black background). The asterisk indicates the tryptophan codon (W) mutated in three nonsense alleles.

(C) Immunoblot analysis of RDE-8, GFP::RDE-8, and GFP::RDE-8(D76N) protein expression. Tubulin was probed as a loading control. Asterisks (*) indicate prominent non-specific bands detected by RDE-8 antibody.

(D) Commassie blue staining of purified wild-type and D76N recombinant RDE-8 proteins.

(E) Denaturing PAGE analysis of recombinant RDE-8 nuclease activity. RDE-8 protein at different concentrations (indicated) was incubated with a 116-nt *sel-1* RNA (nt 414-529) internally labeled with ^{32}P-UTP.

See also Figure S1.

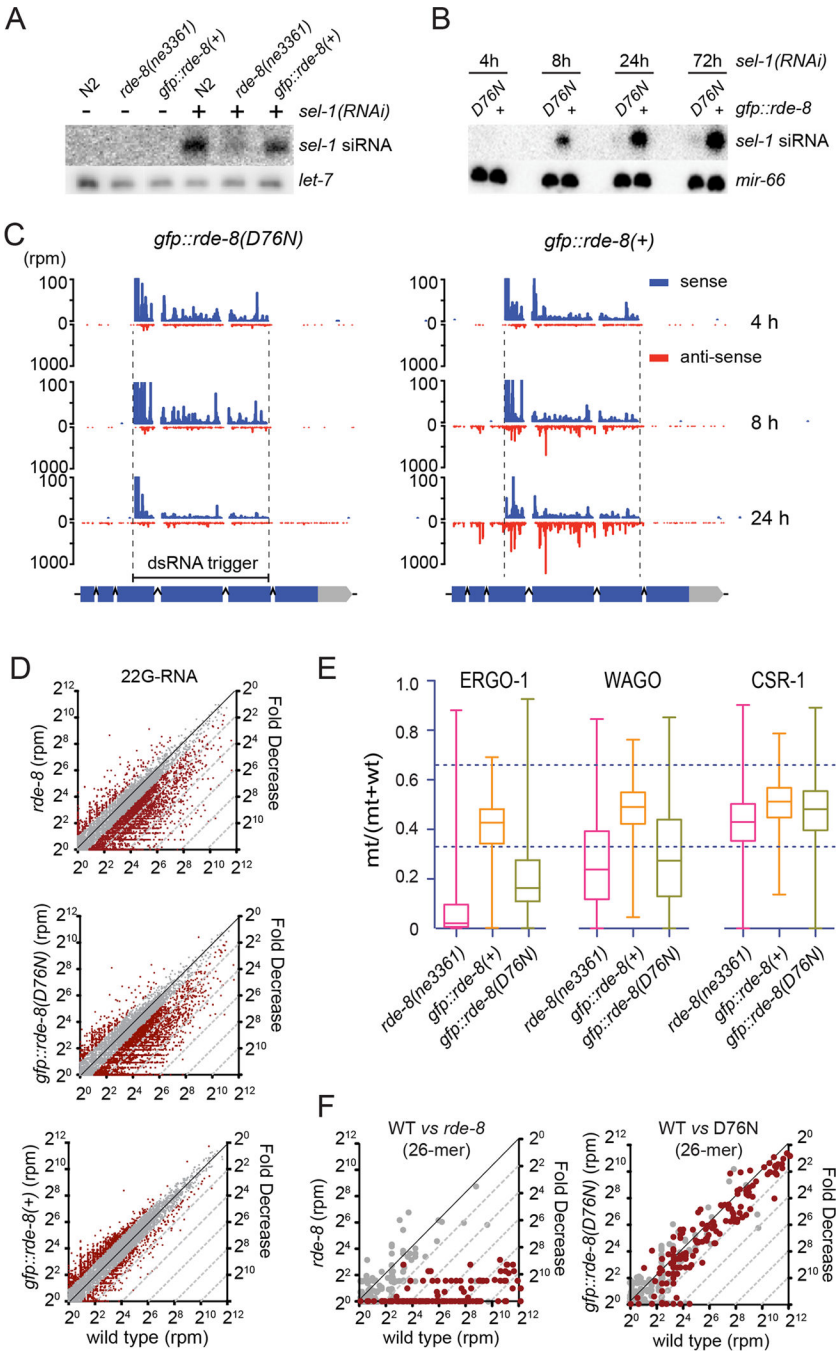

Figure 2. RDE-8 promotes RdRP-dependent small RNA accumulation

(A, B) Northern blot analyses of antisense *sel-1* siRNAs in wild-type, *rde-8* mutant, and mutant transgenic strains (as indicated). The probe hybridizes just upstream (5′) of the *sel-1* dsRNA trigger region (shown in C). *let-7* and *miR-66* miRNAs were probed as loading controls.

(C) Histograms showing sense (blue) and antisense (red) small RNA reads mapping to the *sel-1* gene. Reads were normalized to total non-structural reads. The *sel-1* exons (boxes) and introns (lines) are indicated at bottom; dashed lines delineate the dsRNA trigger region.

(D) Dot plots of endogenous 22G-RNAs targeting annotated genes in *rde-8 (ne3361)* mutant (top) and mutant transgenic strains (as indicated) *gfp::rde-8(D76N)* (middle) or *gfp::rde-8(+)* (bottom) compared to wild type. “rpm” indicates the number of reads per million total reads for a given gene. The black diagonal indicates x=y. Dashed lines (gray) demark regions where loci show the indicated fold decrease of 22G-RNA reads compared to wild type. Gray dots indicate loci that change less than two fold.

(E) Box and whisker plots comparing ERGO-1, WAGO, and CSR-1 pathway 22G-RNAs in *rde-8(ne3361)* mutant (pink) and mutant *gfp::rde-8* transgenic lines (+, orange) and (D76N, green). The ratio of mutant/(mutant + wildtype) are shown. The 75^{th} through 25^{th} percentile are boxed, with the median value shown as a horizontal line within the box. Dashed lines indicate 2-fold enrichment (upper) and depletion (lower).

(F) Dot plots of endogenous 26G-RNA levels in *rde-8 (ne3361)* mutant (left), and mutant *gfp::rde-8(D76N)* transgenic animals (right) compared to wild type. Red dots represent ERGO-1 targets (Vasale et al., 2010) and gray dots represent loci with non-ERGO-1 associated 26-nt antisense reads.

See also Figure S2.

A

Name	Domain/Homology	Coverage (Peptide counts)
RDE-8	RNase_Zc3h12a	57% (154)
NYN-1	RNase_Zc3h12a	44.3% (133)
NYN-2	RNase_Zc3h12a	55.2% (110)
MUT-16	Q/N-rich domain	23.4% (112)
MUT-15	Unknown	55.8% (107)
RDE-3	Nucleotidyltransferase	55.8% (97)
ERI-9	RNase_Zc3h12a	16% (15)

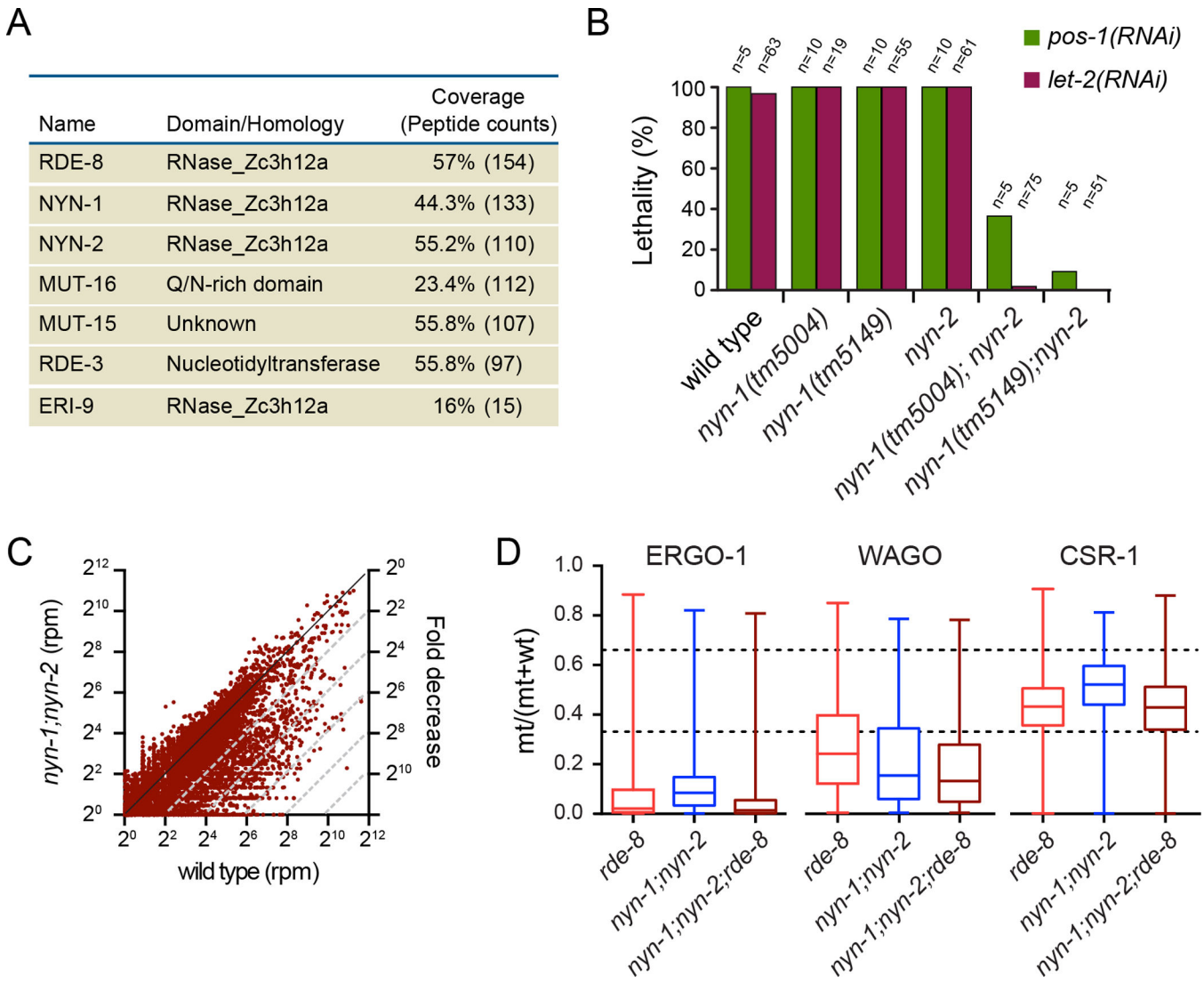

Figure 3. RDE-8 interacts with Mutator components and RDE-8 homologs

(A) Proteins identified by MudPIT analysis of GFP immunoprecipitates from transgenic *gfp::rde-8(+)* worms but not from wild-type worms that do not express GFP::RDE-8. The percent coverage and total number of peptides are indicated for each RDE-8 interactor.

(B) Graphical representation of RNAi sensitivity of wild-type or mutant strains (as indicated). Percent lethal indicates the mean percentage of *pos-1* dead eggs (green bars) or the percentage of *let-2* ruptured or sterile adults observed (red bars). n, number of animals exposed to RNAi.

(C) Dot plots (as described in Figure 2D) of endogenous 22G-RNAs targeting annotated genes in *nyn-1(tm5004); nyn-2(tm4844)* double mutants compared to *wild type*.

(D) Box and whisker plots (as described in Figure 2E) comparing ERGO-1, WAGO, and CSR-1 pathway 22G-RNAs in *rde-8(ne3361)* (orange), *nyn-1(tm5004); nyn-2(tm4844)* double mutants (blue), and *rde-8(ne3361) ;nyn-1(tm5004); nyn-2(tm4844)* triple mutants (brown) relative to wild type.

See also Figure S3.

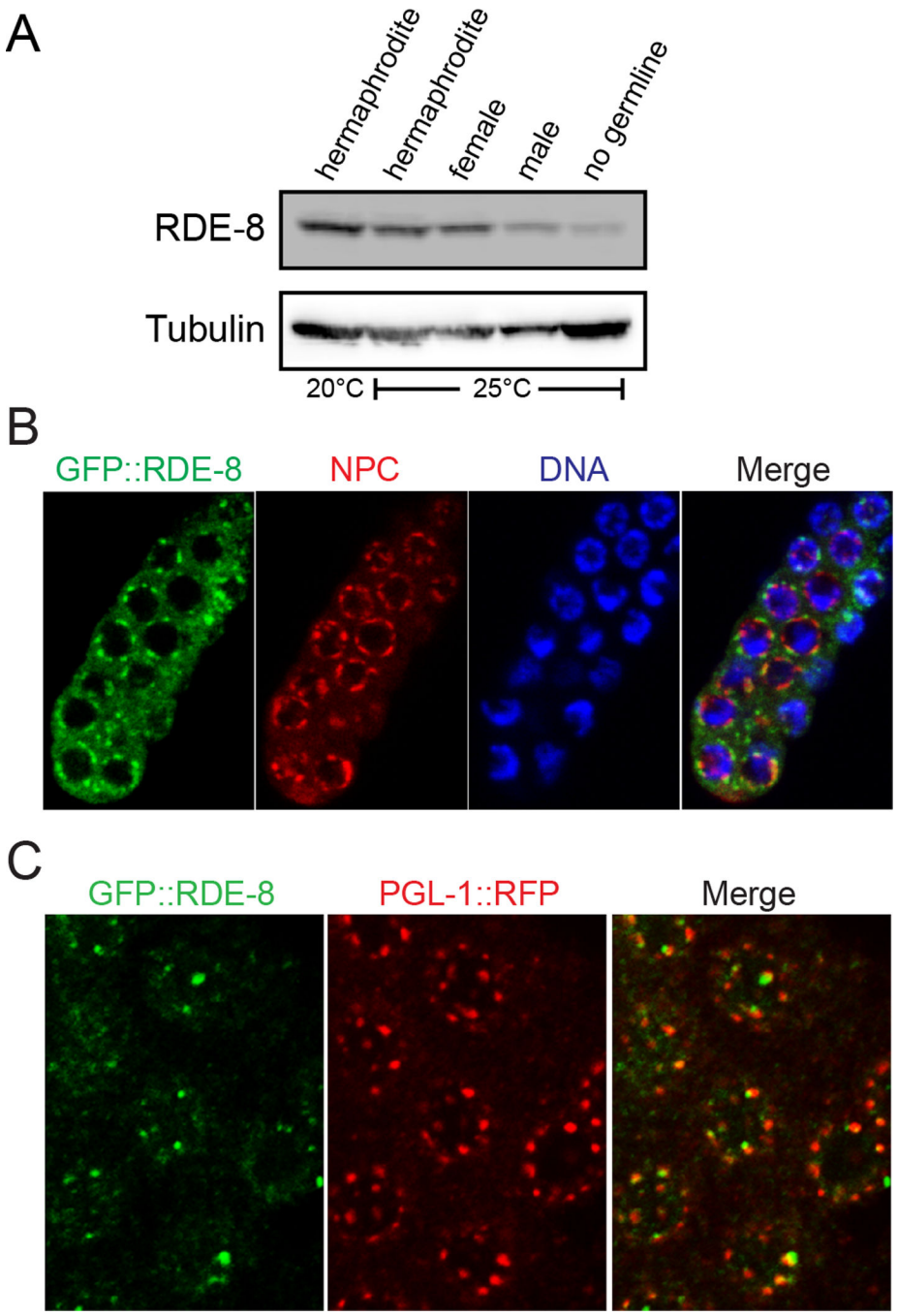

Figure 4. GFP::RDE-8 localizes to perinuclear foci in the germline

(A) Immunoblot analysis of RDE-8 protein from wild-type grown at 20° and 25°C (hermaphrodites), *fem-1(hc17)* grown at 25°C (females), *fog-2(q71)* (males), and from *glp-4(bn2)* animals that lack a germline at 25°C (no germline).

(B, C) Confocal images of dissected gonads. In (B), gonads express GFP::RDE-8 (green) were stained with the MAb414 to detect nuclear pore complex (NPC) proteins (red) and Hoechst to detect DNA (blue). Image overlay at right. In (C), gonads express both

GFP::RDE-8 (green) and the constitutive P-granule component, RFP::PGL-1 (red). Image overlay at right.

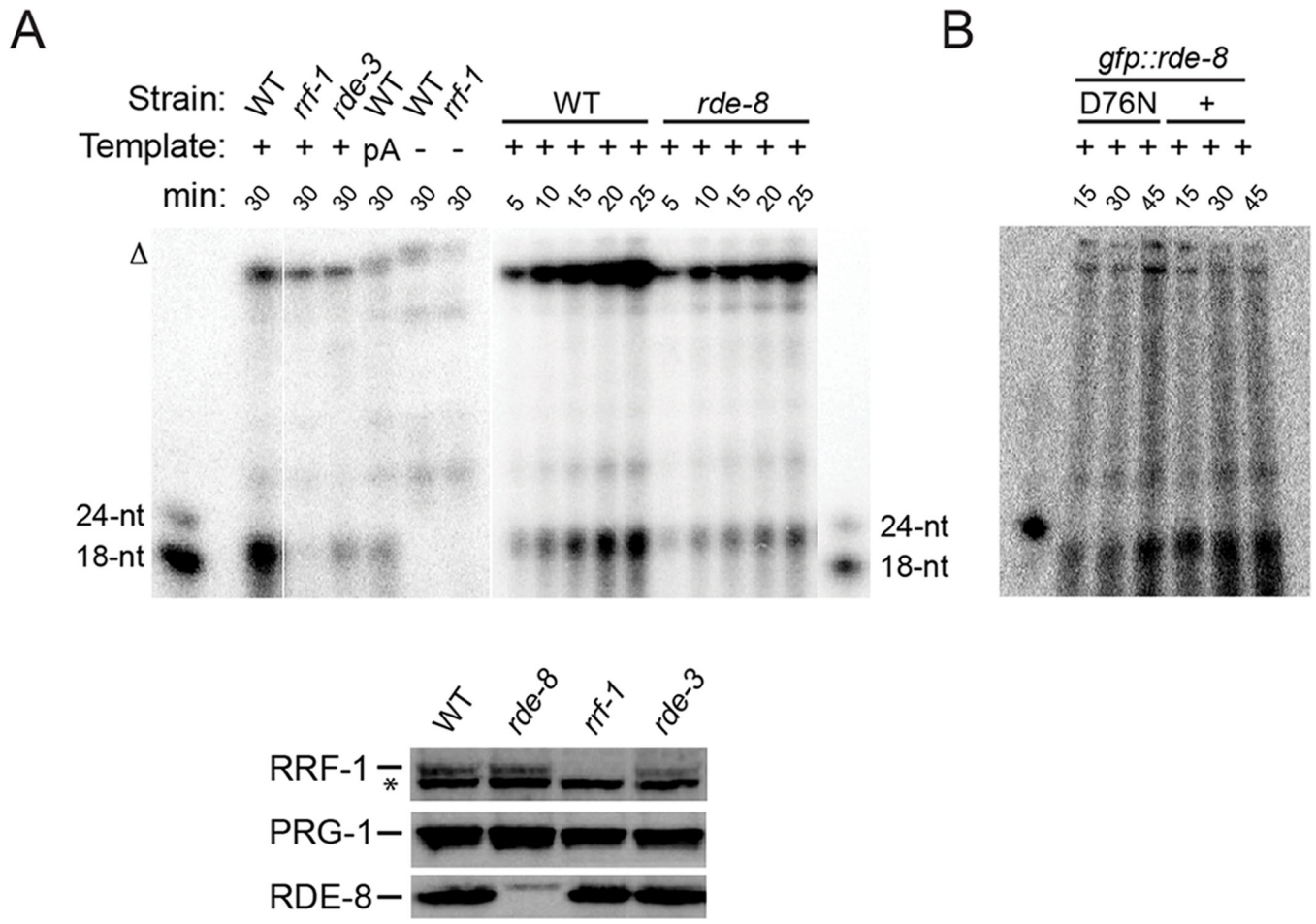

Figure 5. RDE-8 promotes RdRP activity in vitro

(A) Top panel: In vitro RdRP activity assayed in wild-type (WT), *rde-8*(*ne3361*), *rrf-1*(*pk1417*), or *rde-3*(*ne3370*) lysates in the presence (+) or absence (–) of in vitro transcribed and capped RNA template. "pA" denotes that a polyA stretch was added to the 3′ end of the template. Incubation times are indicated in minutes (min). Oligonucleotide size markers are indicated. "Δ" represents uridylated template RNA (Aoki et al., 2008). Bottom panel: Immunoblot analysis of RRF-1, RDE-8, and PRG-1 (loading control) protein levels in lysates used for the RdRP assay.

(B) In vitro RdRP activity assayed in *gfp::rde-8(WT)* and *gfp::rde-8(D76N)* lysates in the presence (+) of in vitro transcribed and capped RNA template, as in (A).

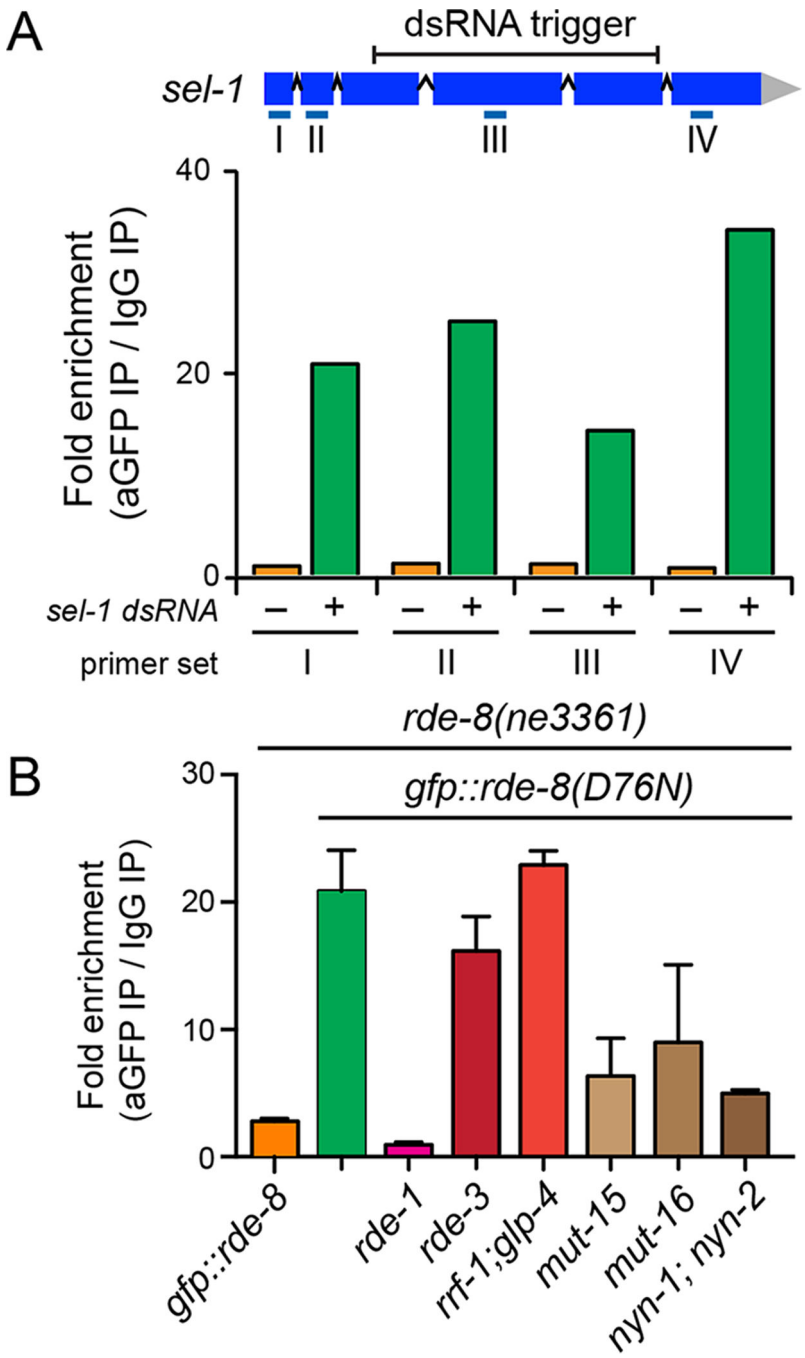

Figure 6. RDE-8 binds target mRNA downstream of RDE-1

(A,B) Bar graphs depicting of RT-qPCR results of *sel-1* mRNA levels in GFP immunoprecipitates divided by levels in control IgG precipitates. All strains assayed were *rde-8(ne3361)* and transgenic for *gfp::rde-8(D76N)* except for one strain that was transgenic for *gfp::rde-8(+)* (orange bar in B). In (A), a schematic diagram of the *sel-1* locus shows the region targeted by dsRNA and the 4 regions assayed by RT-qPCR. In (A), absence of *sel-1* dsRNA (−) served as a specificity control for each region assayed. In (B), all strains were exposed to *sel-1* dsRNA and were assayed for region II.

See also Figure S4.

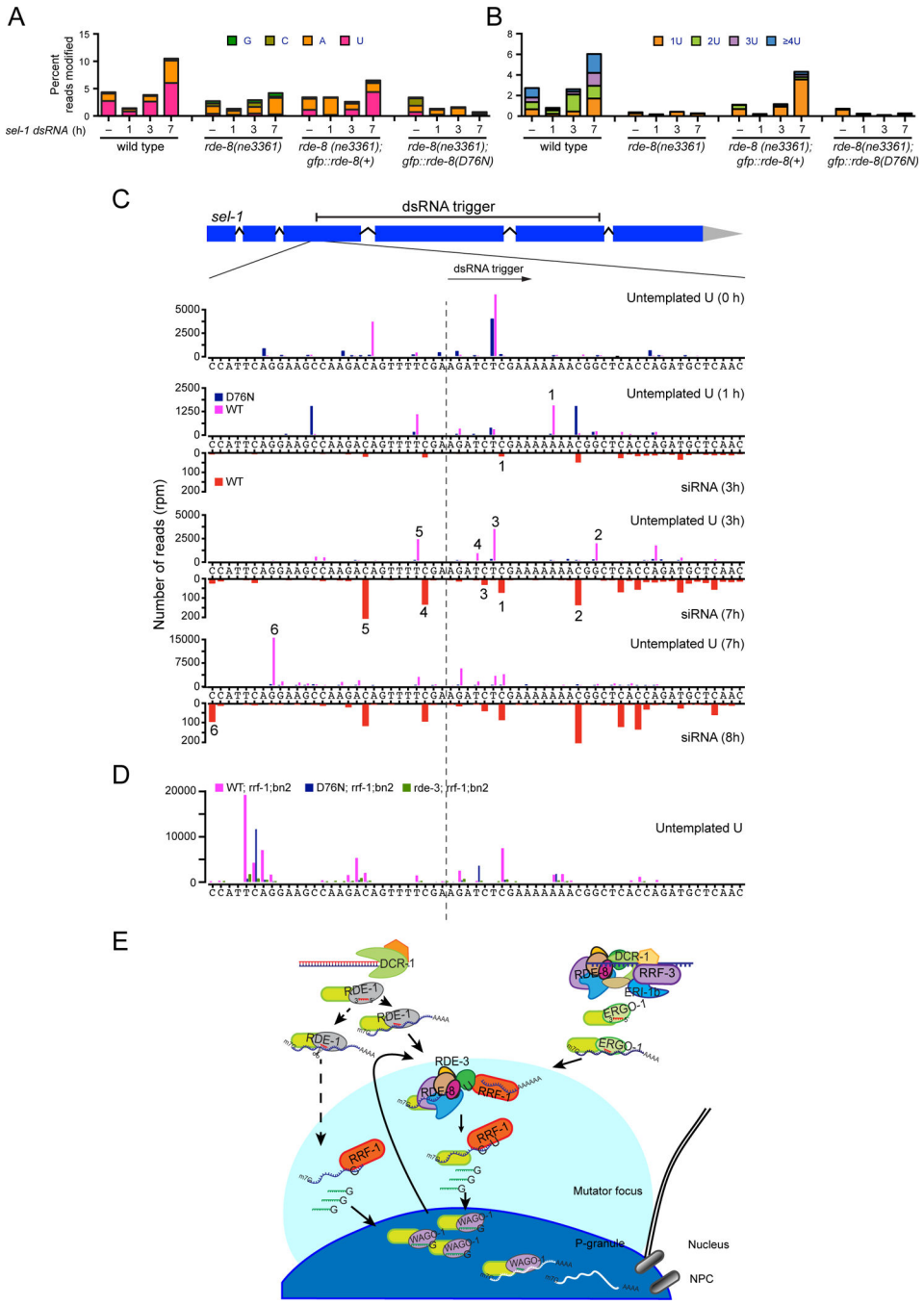

Figure 7. RDE-8 promotes target mRNA cleavage and 3′ uridylation adjacent to sites of secondary siRNA initiation

(A) Bar graphs showing the percentage of untemplated residues detected by 3′ RACE at 3′ ends of *sel-1* mRNA fragments during *sel-1(RNAi)*. Wild-type or *rde-8(ne3361)* animals were exposed to control dsRNA (−) or *sel-1* dsRNA for 1, 3, or 7 hours.

(B) Bar graphs, as in (A), showing the percentage of *sel-1* mRNA fragements with 1, 2, 3, or 4+ untemplated uridine residues during *sel-1(RNAi)*.

(C) Sequence alignment of uridylation sites in wild type (magenta) and D76N (blue) within the region of *sel-1* just 5′ of the dsRNA trigger. 3′ RACE products were sequenced at four time points: prior to dsRNA exposure (0hr) and after 1, 3, or 7 hr (as indicated). The 5′ ends of 22G–siRNAs (plotted below the sequence, orange bars) were identified in the *rde-8(ne3361); gfp::rde-8(+)* transgenic strain. Three time points are shown. The *sel-1* exon (box), intron (line) structure, the dsRNA trigger region, and the region of sequence analyzed are indicated in the schematic.

(D) Sequence alignment, as in (C), showing uridylation sites in RdRP and *rde-3* mutants. The *rrf-1 glp-4(bn2)* background was used to remove RdRP activity in each strain analyzed, including *rde-8(ne3361); gfp::rde-8(+)* (WT, purple), *rde-8(ne3361); gfp::rde-8(D76N)* (D76N, blue) and *rde-3(ne3370)* (green).

(E) Model. See text for details.

See also Figure S6.